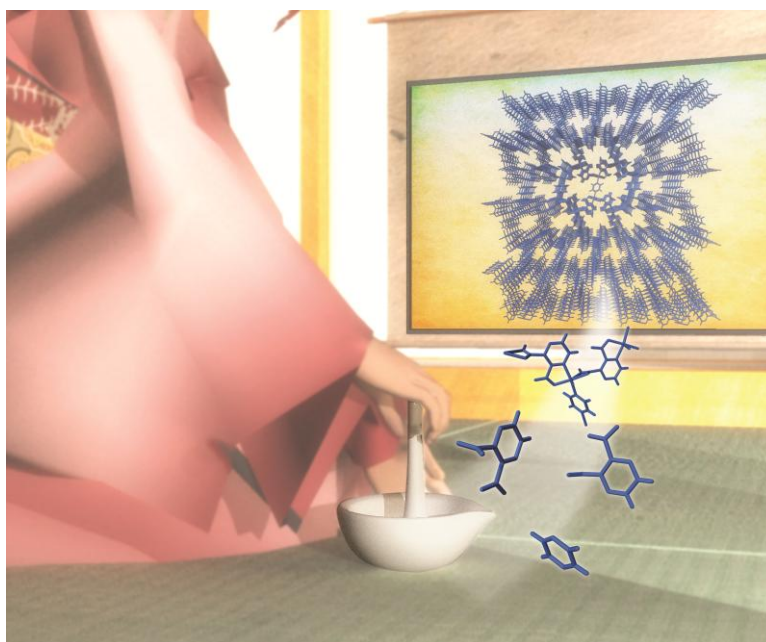


This article is published as part of the *Dalton Transactions* themed issue entitled:

Coordination chemistry in the solid state

Guest Editor Russell E. Morris

Published in [Issue 14, Volume 41](#) of *Dalton Transactions*



Articles in this issue include:

Communications

[Highly oriented surface-growth and covalent dye labeling of mesoporous metal–organic frameworks](#)

Florian M. Hinterholzinger, Stefan Wuttke, Pascal Roy, Thomas Preuße, Andreas Schaate, Peter Behrens, Adelheid Godt and Thomas Bein

Papers

[Supramolecular isomers of metal–organic frameworks: the role of a new mixed donor imidazolate-carboxylate tetradentate ligand](#)

Victoria J. Richards, Stephen P. Argent, Adam Kewley, Alexander J. Blake, William Lewis and Neil R. Champness

[Hydrogen adsorption in the metal–organic frameworks \$\text{Fe}_2\(\text{dobdc}\)\$ and \$\text{Fe}_2\(\text{O}_2\)\(\text{dobdc}\)\$](#)

Wendy L. Queen, Eric D. Bloch, Craig M. Brown, Matthew R. Hudson, Jarad A. Mason, Leslie J. Murray, Anibal Javier Ramirez-Cuesta, Vanessa K. Peterson and Jeffrey R. Long

Visit the *Dalton Transactions* website for the latest cutting inorganic chemistry

www.rsc.org/publishing/journals/dt/

Cite this: *Dalton Trans.*, 2012, **41**, 4027

www.rsc.org/dalton

PAPER

Exploring the coordination chemistry of MOF–graphite oxide composites and their applications as adsorbents

Camille Petit† and Teresa J. Bandosz*

Received 24th October 2011, Accepted 7th January 2012

DOI: 10.1039/c2dt12017h

Metal–organic frameworks (MOFs), besides being porous materials exhibit a very rich chemistry, which can be used for the synthesis of composites and/or the reactive adsorption of toxic gases. In this study, composites of MOFs (MOF-5, HKUST-1 or MIL-100(Fe)) and a graphitic compound (graphite or graphite oxide, GO) were synthesized and tested for the removal of NH₃, H₂S and NO₂ under ambient conditions. The materials were characterized before and after exposure to the target gases by X-ray diffraction, thermogravimetric analysis, N₂ sorption measurement and FT-IR spectroscopy. The results indicate that strong chemical bonds exist between the MOF and GO as a result of the coordination between the GO oxygen groups and the MOFs' metallic centers. Depending on the structure of the MOF, such interactions induce the formation of a new pore space in the interface between the carbon layers and the MOF units, which enhances the physical adsorption capacity of the toxic gases. When unsaturated metallic sites are present in the MOFs, the target gases are also adsorbed *via* coordination to these centers. Further reaction with the framework leads to the formation of complexes. This is accompanied by the collapse of the MOF structure.

Introduction

In the past decades, metal–organic frameworks (MOFs) have drawn a growing interest among the scientific community owing to their high porosity and tunability (both in terms of chemistry and morphology).^{1–3} For this reason, several potential applications have been proposed for these well-defined crystalline networks. They include gas adsorption,^{1,4} gas separation,^{1,4} gas storage,^{1,4} catalysis,^{1,4} drug delivery⁵ and sensing.^{6–10} In particular, many studies devoted to gas adsorption have reported the use of MOFs as separation media. The choice of MOFs as adsorbents is fostered by the large surface areas of these materials with reported values up to 4500 m² g^{−1} for MOF-177¹¹ and large pore space where a significant amount of gas can be stored. However, this apparent high porosity is not without some challenges. Indeed, these materials are full of void space and the ligands do not provide strong dispersive forces, which are needed for the retention of small gas molecules.

Despite their high porosity, MOFs also benefit from a very well-developed chemistry which arises from the presence of metallic sites and functionalized organic ligands. Unlike other adsorbents such as activated carbons, whose main portion consists of

“unreactive” carbon atoms, each unit in a MOF (metals or ligands) can be considered as a potential coordination–adsorption site for the target gas. Consequently, although this aspect tends to be less studied, the chemisorption and/or reactive adsorption of adsorbates on MOFs should be investigated. For instance, studies have reported the coordination of NH₃, NO and H₂ to the unsaturated metallic sites of HKUST-1 (NH₃, H₂),^{12,13} CPO-27-Ni (NO, H₂)^{13,14} and a Cd-containing MOF (H₂).¹⁵ Moreover, Britt and coworkers found that interactions between NH₃ and the amine functionalized ligands in IRMOF-3 could enhance the uptake capacity.¹² Similarly, in the study by Demessence and coworkers, the high CO₂ adsorption on a Cu-containing MOF was partly attributed to the interactions of the species with the amine groups of the organic ligands.¹⁶ Some evidence of hydrogen bonding between NH₃ and the metal oxide units of MOF-5 has also been reported.¹⁷ Considering all these findings, it is important to investigate the potential interactions between the adsorbate and the framework and analyze whether the binding of the adsorbate to the various MOF reactive sites can affect the stability of the framework. In particular, a potential “risk” would be the weakening of the coordination link between the metal and the organic ligand.

Another aspect of the coordinative chemistry of MOF materials is the formation of MOF-based composites. The reasons for synthesizing such materials usually include a better water-stability, an increased adsorption uptake, or the formation of user-friendly materials (*e.g.*, thin films, membranes). Several research groups have reported the formation of such materials in which chemical bonds between the MOF and the other substrate are involved.^{18–20} For instance, Jahan and coworkers reported

The Department of Chemistry, The City College of New York and the Graduate School of the City University of New York, 160 Convent Avenue, New York, USA. E-mail: tbandosz@ccny.cuny.edu; Fax: +1 212-650-6107; Tel: +1 212-650-6017

† Present address: The Department of Chemical Engineering and Earth and Environmental Engineering, Columbia University, 500 West 120th street, New York, USA.

the binding of MOF-5 to COOH-functionalized graphite.¹⁸ Shekka and coworkers showed that copper ions in a Cu-based MOF could be used as linkers between the carboxyl groups of SAMs and those of the organic ligands.¹⁹ In a different study, Hermes and coworkers described the growth of MOF-5 crystals on COOH-functionalized SAMs as well as alumina.²⁰ In prior studies, we reported the formation of MOF-graphite oxide (GO) composites *via* interactions between the oxygen groups of GO and the metallic centers of the MOF.^{21,22}

In this paper, we present an overview of the coordination chemistry of MOF units: (i) as a component of composite materials and (ii) as gas adsorbents. The influence of this coordination on the materials' structure, porosity, crystallinity, thermal and chemical stabilities, and adsorption capacity was investigated. For this study, three different MOFs were selected: MOF-5, HKUST-1 and MIL-100(Fe). These frameworks were used in the synthesis of composites with graphite oxide and graphite. The materials were tested as NH₃, H₂S and NO₂ adsorbents. Although some data were already reported in our prior studies,^{17,21–27} we combine relevant results in this paper in order to highlight characteristic features of the MOFs' chemistry for both the formation of composites and the reactive adsorption of gases.

Experimental

Materials

Graphite oxide and graphite. Graphite oxide was prepared using the Hummers method²⁸ as described in ref. 29. Briefly, graphite powder (Sigma-Aldrich) was oxidized using sulfuric acid, potassium permanganate and hydrogen peroxide at room temperature. The mixture was left overnight and GO particles were separated from the excess liquid by decantation followed by centrifugation. The remaining suspension was subjected to dialysis until no precipitate of BaSO₄ was detected by addition of BaCl₂. Then, the wet form of graphite oxide was centrifuged and freeze-dried. A fine brown powder of the initial graphite oxide was obtained. The resulting material is referred to as GO.

The graphite sample used in this study was synthetic graphite supplied by Asbury Graphite Mills. It was used as received and is referred to as G.

Zn-based materials. The Zn-containing MOF selected was MOF-5. It contains zinc oxide tetrahedra connected by benzene dicarboxylate (BDC) ligands. The structure has been fully described by Li and coworkers³⁰ and the details of the synthesis procedure can be found elsewhere.²¹ Briefly, MOF-5 was prepared by mixing zinc nitrate hexahydrate and 1,4-benzenedicarboxylate (BDC) in *N,N*-dimethylformamide (DMF) until complete dissolution of the solids. Then, the mixture was heated at 115–120 °C for 24 h. After cooling, the crystals formed were collected, washed with DMF, and immersed in fresh chloroform. The chloroform was changed twice during two days. Finally, the crystals were collected and heated at 130–135 °C for 6 h under vacuum. The resulting material was then kept in a desiccator and is referred to as MOF-5.

The composite material was prepared by dispersing GO powder in the well-dissolved zinc nitrate–BDC mixture and the

resulting suspension was subsequently subjected to the same synthesis procedure as for MOF-5.²¹ The added GO consisted of 10 wt% of the final material. The resulting sample is referred to as ZnMGO.

Cu-based materials. The Cu-containing MOF material selected was a copper-based MOF with copper ions as the metallic component and benzene tricarboxylate (BTC) as the organic bridges. This material is commonly referred to as HKUST-1 and its structure has been investigated in detail by Chui and coworkers.³¹ The synthesis of HKUST-1 was conducted as described in ref. 22, following a procedure adapted from Millward and coworkers' method.³² Briefly, HKUST-1 was prepared by dissolving copper nitrate hemipentahydrate and 1,3,5 benzenetricarboxylic acid (BTC) in a mixture of DMF, ethanol and deionized water. The mixture was subjected to stirring and sonication to ensure complete dissolution of the crystals. The mixture was then heated at 85 °C under shaking for about 20 h. After cooling, the crystals were filtered, washed and immersed in dichloromethane. Dichloromethane was changed twice during three days. Finally, the crystals were collected and dried under vacuum at 170 °C for 28 h. The resulting product was kept in a desiccator and is referred to as HKUST-1.

The composite material with GO was prepared by dispersing GO powder in the well-dissolved copper nitrate–BTC mixture. The resulting suspension was then subjected to the same synthesis procedure as for HKUST-1, as described in ref. 22. The added GO consisted of about 10 wt% of the final material. The resulting sample is referred to as CuMGO.

The same procedure as for CuMGO was used to synthesize the composite material with graphite.²⁷ The added graphite consisted of about 10 wt% of the final material. The resulting sample is referred to as CuMG.

Fe-based materials. MIL-100(Fe) was selected for this study. This MOF consists of iron(III) ions connected *via* BTC organic bridges. The resulting network exhibits a zeolite-like morphology.³³ The synthesis of this MOF was adapted from that reported by Horcajada and coworkers³³ and the details of the procedure can be found in ref. 26. Briefly, iron powder, BTC, hydrofluoric acid, nitric acid and deionized water were mixed, stirred and placed in a Teflon liner. The liner was then inserted in an acid digestion vessel (Parr Instrument) and then progressively heated to 150 °C within 8 h. The temperature was maintained at 150 °C for 4 days and then the vessel was progressively cooled to room temperature (in about 24 h). The crystals formed were collected and washed with deionized water. The sample was subsequently immersed in hot water (80 °C) for 3 h. The product was finally filtrated and dried overnight in air at 120 °C. The synthesized MOF was kept in a desiccator and is referred to as MIL.

The composite material with Fe was prepared in the same way as for MIL except that GO powder was added to the mixture of MOF precursors and the mixture was subsequently sonicated before the heat treatment.²⁶ The composite contains 9 wt% GO and is referred to as FeMGO.

Methods

NH₃, NO₂ and H₂S breakthrough dynamic tests. In order to determine the breakthrough capacities of the materials studied, dynamic breakthrough tests were performed at room temperature. NH₃ adsorption was tested on all materials whereas NO₂ and H₂S adsorptions were tested only on GO, HKUST-1 and CuMGO. In a typical test, a flow of gas (NH₃, H₂S or NO₂) diluted with air went through a fixed bed of adsorbent. The total inlet flow rate was 225 mL min⁻¹ for NO₂ and NH₃ tested on Cu and Fe-based materials, 250 mL min⁻¹ for H₂S and 450 mL min⁻¹ for NH₃ tested on Zn-based materials. The concentration of each species in the inlet stream was 1000 ppm. The adsorbent's bed contained about 2 cm³ of glass beads well mixed with the amount of adsorbent required to obtain a homogeneous bed with minimum pressure drop. In the case of Zn-based materials, the bed consisted of 2 cm³ of adsorbent only (no glass beads). The concentration of gas (NH₃, H₂S or NO₂) in the outlet stream was measured using an electrochemical sensor (Multi-Gas Monitor ITX system for NH₃ adsorption and Multi-Gas Monitor RAE system for H₂S and NO₂ adsorptions). The adsorption tests were stopped when the outlet gas concentration reached the upper limit of the sensor (100 ppm for NH₃ and H₂S and 20 ppm for NO₂). The adsorption capacity of each adsorbent was calculated in mg per gram of the material by integration of the area above the breakthrough curve. For NH₃ and NO₂ adsorption tests, the gas was diluted in dry air whereas for H₂S, only dilution in moist air was performed. The presence of water is crucial to the adsorption of H₂S as shown in previous works,³⁴ and that is why the uptake of H₂S was tested only in the presence of humidity. Moreover, in the latter case, the adsorbent bed was prehumidified prior to running the breakthrough tests. In all cases, after the breakthrough tests, all samples were exposed to a flow of carrier air only to impose the desorption of the target gas and thus to evaluate the strength of its retention. The air flow was 180 mL min⁻¹ for NO₂ and NH₃ with Cu and Fe-based materials, 225 mL min⁻¹ for H₂S, and 360 mL min⁻¹ for NH₃ with Zn-based materials.

In the case of NO₂ adsorption, nitrogen monoxide (NO) concentration in the outlet stream was also monitored. NO is often encountered as a by-product^{35,36} and, although less toxic than NO₂, its presence is not a desired feature and must be controlled.

Sorption of nitrogen. Nitrogen isotherms were measured at -196 °C using an ASAP 2010 instrument (Micromeritics). Prior to each measurement, initial and exposed samples were outgassed at 120 °C to constant vacuum (10⁻⁵ Torr). The surface area, *S*_{BET} (Brunauer-Emmet-Teller method),³⁷ the micropore volume, *V*_{mic} (calculated from the t-plot),³⁸ the mesopore volume, *V*_{mes}, the total pore volume, *V*_t, were calculated from the isotherms.

FT-IR spectroscopy. Fourier transform infrared (FT-IR) spectroscopy was carried out with a Nicolet Magna-IR 830 spectrometer using the attenuated total reflectance (ATR) method for the NH₃ and H₂S-related samples and the diffuse reflectance method for the NO₂-related samples. The latter method was used to avoid damage of the ATR crystal owing to the strong oxidizing nature of NO₂. The spectrum was generated, collected 16 times and corrected for the background noise. For the NH₃ and

H₂S-related samples, the experiments were done on the powdered materials without KBr addition. For the NO₂-related samples, the powdered materials (2–3 wt%) were mixed with KBr (97–98 wt%).

Thermal analysis. Thermogravimetric (TG) curves were obtained using a TA Instrument thermal analyzer. The initial and exposed samples were subjected to an increase in temperature (10 °C min⁻¹) while the nitrogen flow rate was held constant (100 mL min⁻¹). From the TG curves, the differential TG (DTG) curves were derived.

X-ray diffraction. X-ray diffraction (XRD) measurements were conducted using standard powder diffraction procedures. Adsorbents were ground with DMF (methanol for GO) in a small agate mortar. The mixture was smear-mounted onto a glass slide and then analyzed by Cu K_α radiation generated in a Philips X'Pert X-ray diffractometer. A diffraction experiment was run on standard glass slide for the background correction.

Results and discussion

The XRD patterns of the different materials studied are reported in Fig. 1.^{21,22,26,27} GO and G exhibit the expected pattern for graphitic materials with a single peak at 2 Theta ~10.2° and 26°, respectively. From these peaks, the interlayer distances (*d*₀₀₂) are calculated and correspond to 8.7 and 3.4 Å, respectively. These distances are in the range of those usually observed for graphite oxide and graphite.^{39–41} In the case of the Zn- and Cu-based composites, the XRD peaks from the parent MOFs are preserved suggesting that the graphitic component did not disturb the crystallization of the MOF-5 and HKUST-1 structures. This is not the case for FeMGO sample, for which most of the peaks pertaining to the parent MOF are missing. For this composite, the carbon layers from GO likely prevented the proper assembly of the MOF units. It is interesting to notice that the (002) peak of GO is not observed on the spectra of the ZnMGO, CuMGO and FeMGO composites. This is related to the exfoliation/dispersion of GO in the polar solvents used during the material synthesis. On the contrary, graphite, owing to its hydrophobic nature, could not fully disperse and thus agglomerates of graphene layers are still present in CuMG as indicated by the graphite diffraction peak on the XRD spectrum of the composite.

Although the MIL-100 structure in FeMGO did not crystallize properly, the MOF units are still formed as confirmed by thermal analysis. As seen in Fig. 2, FeMGO exhibits the same peaks as those of MIL (three peaks at 410 °C, 490 °C and 600 °C).²⁶ Similarly, ZnMGO, CuMGO and CuMG samples have the same thermal decomposition pattern as that of their parent MOF.^{17,22,27} In the case of MOF-5 and HKUST-1 as well as their composites, this decomposition occurs in one step and is related to the degradation of the organic ligands with release of CO₂.^{42,43} For MIL and FeMGO, the DTG peaks are assigned to the decomposition of the organic ligand (270 °C) followed by the reduction of the species from Fe₃O₄ to Fe₂O₃ and finally FeO.^{33,44,45} For the composites with GO, it is interesting to observe that the main peak related to GO at 200 °C, which corresponds to the decomposition of the epoxy groups,⁴⁶ is missing. This indicates that the epoxy groups are involved in the building

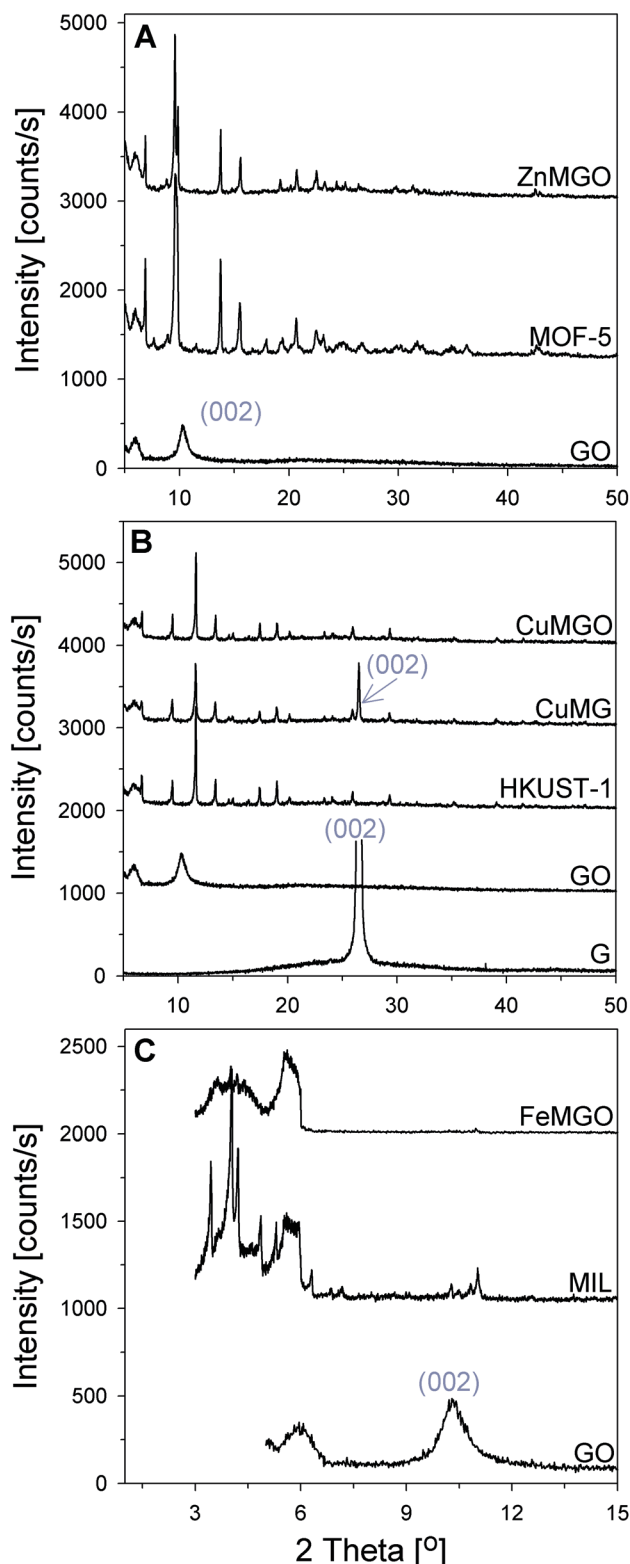


Fig. 1 XRD spectra of the initial adsorbents: (A) GO and Zn-based materials, (B) G, GO and Cu-based materials, and (C) GO and Fe-based materials.

process of the composites. More generally, the functional groups in GO are coordinated to the metallic sites of the MOFs forming a uniform new material.

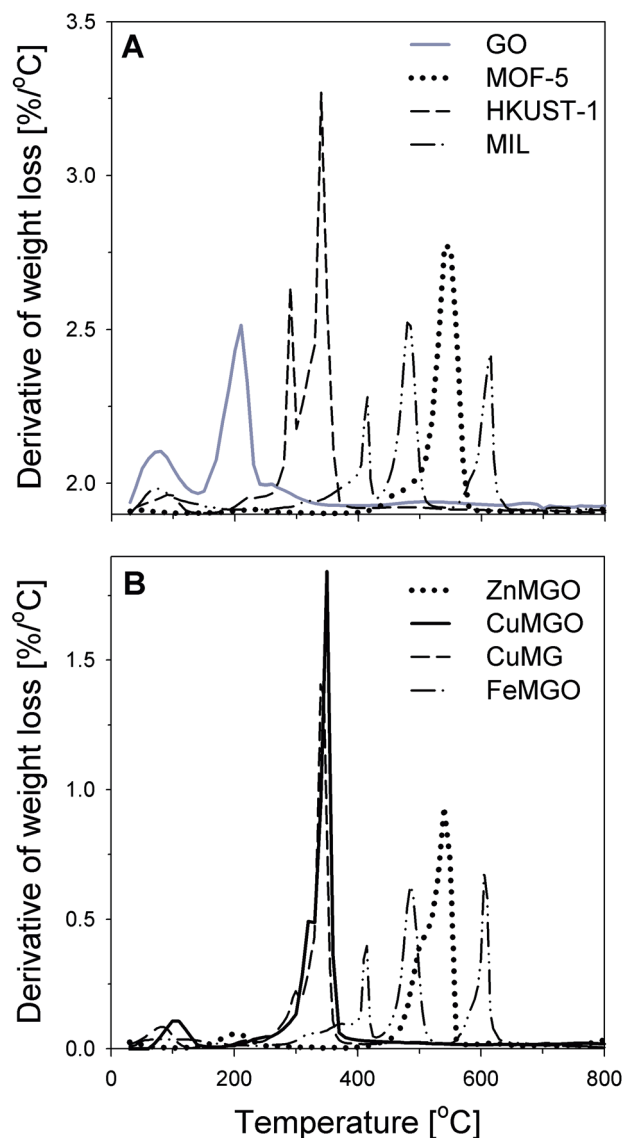
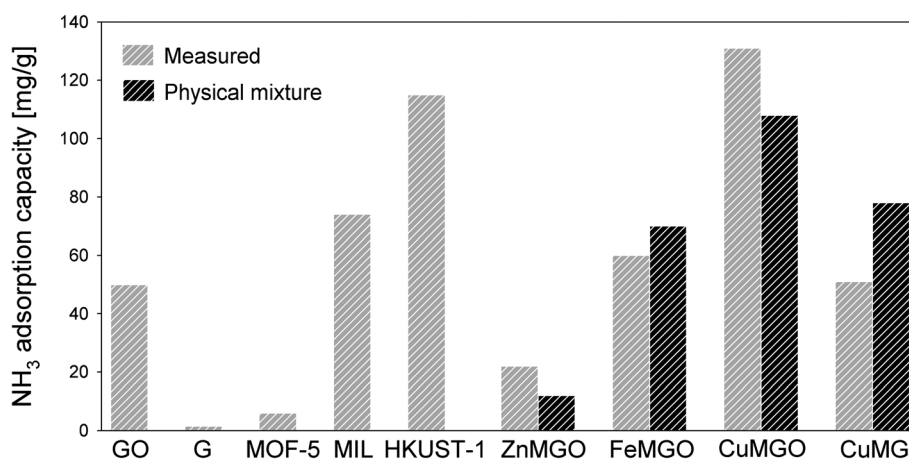


Fig. 2 DTG curves of the initial adsorbents: (A) parent materials, and (B) composites.

The chemical links between GO and the MOF units enable the formation of a new pore space at the interface between the two composite components, as confirmed by the parameters of porous structure reported in Table 1.^{21,22,26,27} Indeed, an enhancement in the porosity and surface area is observed with ZnMGO and CuMGO compared to the hypothetical values calculated assuming the physical mixture of the composite components. It is anticipated that in this new pore space, the dispersive forces are stronger owing to the dense nature of the graphene layers compared to the MOF units. For CuMG, since graphite is deprived of any functional groups, there is no possible coordination between HKUST-1 and G and the porosity is similar to that calculated for a physical mixture of the two materials. In the case of FeMGO, the situation is different since the porosity of the composites decreased compared to that of the physical mixture. This observation does not question the existence of links between GO and MIL units but rather suggests that

Table 1 Parameters of the porous structure calculated from nitrogen adsorption isotherms at $-196\text{ }^\circ\text{C}$ for the initial samples and the parameters calculated for the hypothetical physical mixtures (H). The MOF content of each composite is listed in parenthesis

Sample	S_{BET} ($\text{m}^2\text{ g}^{-1}$)	V_t ($\text{cm}^3\text{ g}^{-1}$)	V_{mic} ($\text{cm}^3\text{ g}^{-1}$)	$S_{\text{BET}H}$ ($\text{m}^2\text{ g}^{-1}$)	V_tH ($\text{cm}^3\text{ g}^{-1}$)	$V_{\text{mic}H}$ ($\text{cm}^3\text{ g}^{-1}$)
G	Nil	Nil	Nil	—	—	—
GO	Nil	Nil	Nil	—	—	—
MOF-5	793	0.408	0.385	—	—	—
HKUST-1	909	0.471	0.449	—	—	—
MIL	1413	0.746	0.587	—	—	—
ZnMGO (10 wt%)	806	0.416	0.388	714	0.367	0.315
CuMG (10 wt%)	912	0.471	0.444	818	0.424	0.404
CuMGO (10 wt%)	1002	0.527	0.478	818	0.424	0.404
FeMGO (9 wt%)	1172	0.600	0.501	1290	0.680	0.536

**Fig. 3** NH_3 adsorption capacities for the various adsorbents tested: G, GO, the Zn-, Cu-, and Fe-based materials.

the coordination between the two parent materials was not beneficial. This is related to the spherical structure of the MIL units which, unlike MOF-5 and HKUST-1 whose configurations are cubic, prevents the formation of MIL network by blocking the assembly of additional MIL units once GO layers are attached, as explained in ref. 26. This phenomenon also explains the poor crystallization of MIL-100 in FeMGO observed *via* XRD.

The materials were tested for the removal of NO_2 , NH_3 and H_2S molecules.^{17,23–27} Although the molecules of all these species have a small kinetic diameter (between 3.0 and 3.6 Å),^{47,48} their chemical properties differ significantly (*e.g.*, acid–base and redox properties). Adsorbents are usually designed for a given adsorbate or type of adsorbate (*e.g.*, bases *vs.* acids), and it is thus interesting to evaluate whether MOFs can exhibit features that would satisfy the requirements for the retention of a wider variety of species. The adsorption capacities of the parent materials and the composites are reported in Fig. 3 and Fig. 4.^{17,23–27} The measured uptakes of the composites are compared to those calculated for a physical mixture of the graphitic component (G or GO) and the MOF taking into account their composition. Such a comparison enables the identification of a synergistic effect. As seen in Fig. 3, GO adsorbs a large amount of ammonia owing to the presence of oxygen groups on the surface of the basal planes able to react with the gas.⁴⁹ On the contrary, the adsorption capacity of G is low owing to the lack of these groups. MOF-5, unlike HKUST-1 and MIL,

exhibits a small adsorption capacity. This is because, all metallic sites of this material are saturated and only physisorption can occur. On the contrary, for the two other MOF samples, ammonia can bind to the unsaturated metallic sites and/or the water molecules already binding to the metallic centers. This process is explained in more detail below. As seen in Fig. 3, the adsorption capacities of ZnMGO and CuMGO are higher than those calculated for the corresponding physical mixtures. This indicates the presence of a synergistic effect which must be related to the presence of the new pore space in the interface between MOF units and GO as described above. On the contrary, the CuMG and FeMGO samples do not exhibit any enhancement in porosity. Once again, this is evidence that there are no beneficial interactions between the graphitic component of these materials and the MOF units. It is worth mentioning that CuMGO is a better ammonia adsorbent than both HKUST-1 and GO and its capacity exceeds most of those reported in the literature on other adsorbents.^{49–51} The synergistic effect observed for ammonia adsorption on CuMGO is also visible for both NO_2 and H_2S adsorptions on the same composite, as seen in Fig. 4. Once again, such an enhancement in adsorption capacity is linked to the new porosity created in the interface where dispersive forces are the strongest. Although only one composite per type of MOF has been presented in this study, several composites with various MOF and GO contents were prepared and tested for gas adsorption as reported in ref. 17 and ref. 23–26. Considering this larger array of materials, the trends described in

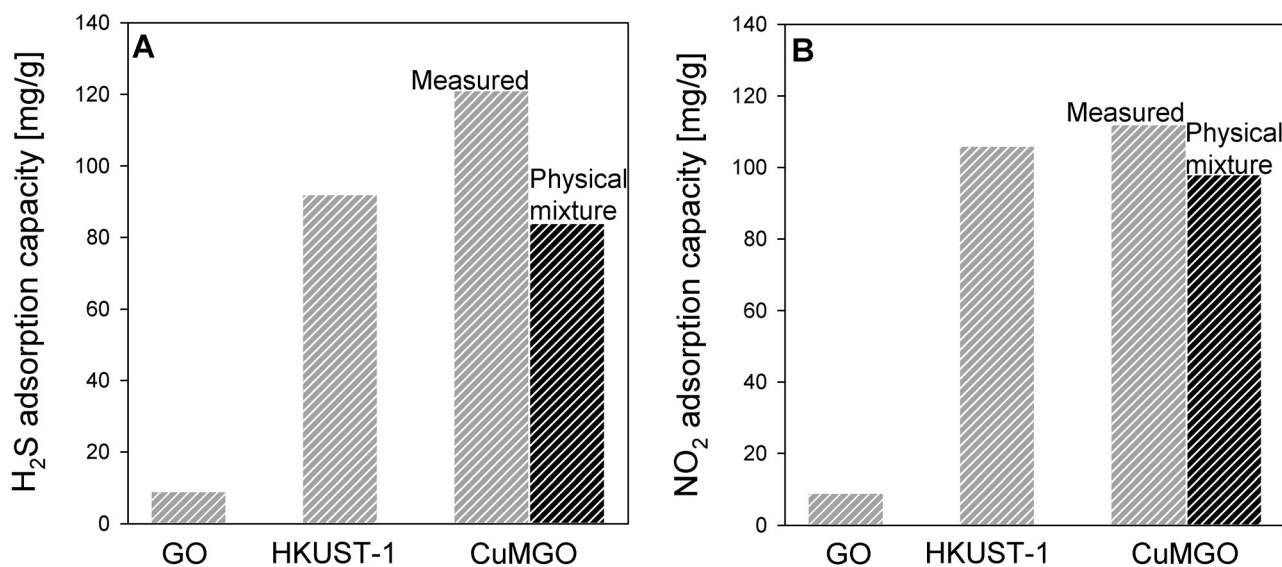


Fig. 4 Comparison of (A) H₂S and (B) NO₂ adsorption capacities for the GO and the Cu-based materials.

the current paper are supported by the results obtained on other composites.

Although physisorption is an apparent mechanism of adsorption on the MOFs and the derived composites, it does not solely control the whole adsorption process. Indeed, so far, the porosity of the composites in comparison to that calculated for the physical mixture was used to qualitatively explain the trend observed in the adsorption capacity, and especially to justify the existence or not of a synergetic effect. However, such explanation does not address the quantitative values of adsorption capacity. For instance, despite the fact that the creation of new pores with strong dispersive forces visibly increases the gas uptake, there is no quantitative correlation between the porosity and/or surface area and the breakthrough capacities of the studied MOFs and composites. Although MIL and FeMGO have a higher porosity than HKUST-1 and CuMGO, their NH₃ adsorption capacity is still smaller. More importantly, visible signs of reactive adsorption were observed during the breakthrough tests *via* the color change of the adsorbent. During NH₃, NO₂ and H₂S adsorptions on HKUST-1, CuMGO and CuMG, the materials, initially dark blue, turned light blue. With the progress of the adsorption test, the color of the adsorbent further changed to another light blue or blackish tint during exposure to NH₃ and H₂S, respectively. In the case of NO₂ adsorption, only the first color change was observed. This first color change is attributed to the coordination of the gas molecules to the MOF Cu sites. This phenomenon has already been reported by other researchers and it is related to the presence of a lone pair of electrons on the adsorbate molecules which can bind to the metallic centers.¹² In this first step, the ability of NH₃, H₂S and NO₂ to act as ligands and coordinate the metallic centers seems to prevail over the distinct acid–base and redox properties of these species. The second color change is likely caused by the formation of new complexes as a result of the reaction of NH₃ or H₂S with the HKUST-1. In particular, the dark tint of the adsorbent after H₂S adsorption is assigned to the formation of CuS. Thermal studies of the exposed materials reported below provide support for this hypothesis.

To investigate in more detail the mechanisms of reactive adsorption of the various gases on the different materials tested, the exposed samples were characterized by FT-IR spectroscopy, thermogravimetric analysis and N₂ sorption and the results were compared to those obtained on the unexposed materials. FT-IR spectra for the initial and exposed composites are shown in Fig. 5.^{17,23–27} The results for HKUST-1, MOF-5 and MIL are not presented here for the sake of clarity but the conclusions drawn below also apply to these materials since the composites mostly consist of the MOF units. Only the wavenumber range 600–1800 cm⁻¹ is presented since it contains the most relevant features. The initial spectra of all composites exhibit similar bands corresponding to the symmetric (1370, 1450 cm⁻¹) and asymmetric (1590, 1645 cm⁻¹) vibrations of the carboxylate groups of the organic ligand,^{52–54} as well as its out of plane vibrations (below 1300 cm⁻¹).^{54,55} The vibration bands related to the functional groups in GO are not seen owing to the rather small content of this material in CuMGO. Upon exposure to NH₃, NO₂ or H₂S, noticeable changes are observed in the region 1100–1800 cm⁻¹ of both CuMG and CuMGO spectra. They indicate a modification of the carboxylate environment likely caused by a different coordination to the Cu sites. In fact, some of the new bands appearing on the spectra of the exposed samples are observed on the spectrum of BTC (spectrum shown in Fig. 5(A)), as, for instance, at 1605 cm⁻¹ and/or 1240 cm⁻¹. This indicates that the MOF units reacted with the target adsorbates causing the release of the ligands (not linked to the metallic sites any more). In the case of H₂S adsorption on CuMGO, the appearance of a broad band around 1705 cm⁻¹ indicates the protonation of the carboxylate groups in BTC as a result of their reaction with H₂S. On the contrary, for NH₃ and NO₂ adsorption, the ligands likely remained in their basic form. Unlike for the Cu-based materials, the spectra for the exposed Zn- and Fe-based samples exhibit the same features as those of the initial samples. This indicates that the framework did not react with the adsorbates or at least not in a way that would modify the coordination of the organic ligands. In fact, since in MOF-5 and

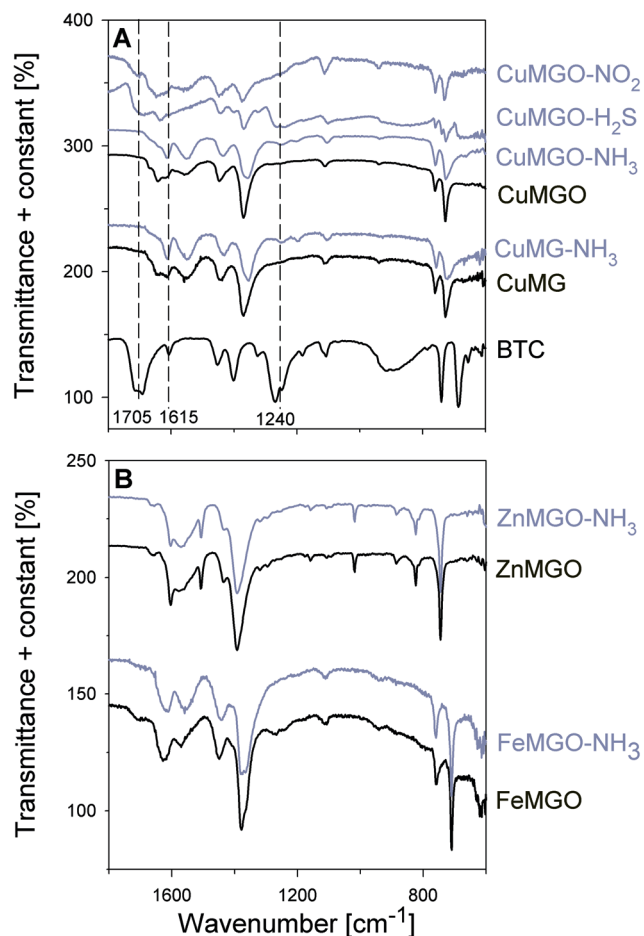


Fig. 5 FT-IR spectra for the initial and exposed samples: (A) Cu-based composites, and (B) Zn- and Fe-based composites.

ZnMGO, the metallic centers are saturated, ammonia cannot directly bind to the Zn sites and only hydrogen bonding with the oxygen atoms of the ZnO_4 units is possible as described in another study.¹⁷ In the case of MIL and FeMGO, the Fe sites are already interacting with water molecules. Consequently, the envisioned reactive pathway is the acid–base reaction between ammonia and water, which has been described in more detail in ref. 26.

Some indication of the nature of the products of reactive adsorption in the Cu-based materials is obtained by running the thermogravimetric analysis of the exposed samples.^{17,23–26} The results are presented in Fig. 6. In the range 175–275 °C, broad peaks appear after exposure to the adsorbates. Given the composition of HKUST-1, the nature of the adsorbates as well as the temperature range, it is proposed that these new peaks correspond to the decomposition of $\text{Cu}(\text{NH}_3)_4^{2+}$, CuS and $\text{Cu}(\text{NO}_3)_2$, formed during the adsorption of NH_3 , H_2S and NO_2 , respectively.⁵⁶ The formation of $\text{Cu}(\text{NO}_3)_2$ has been explained in detail in a prior study²⁵ and is supported by the detection of NO released during the process. In the case of ammonia adsorption, there is no direct evidence for the presence of $\text{Cu}(\text{NH}_3)_4^{2+}$ and further tests would be required to confirm the formation of this specific complex. The release of the organic ligands in the Cu-based materials is supported by the broadening of the peak

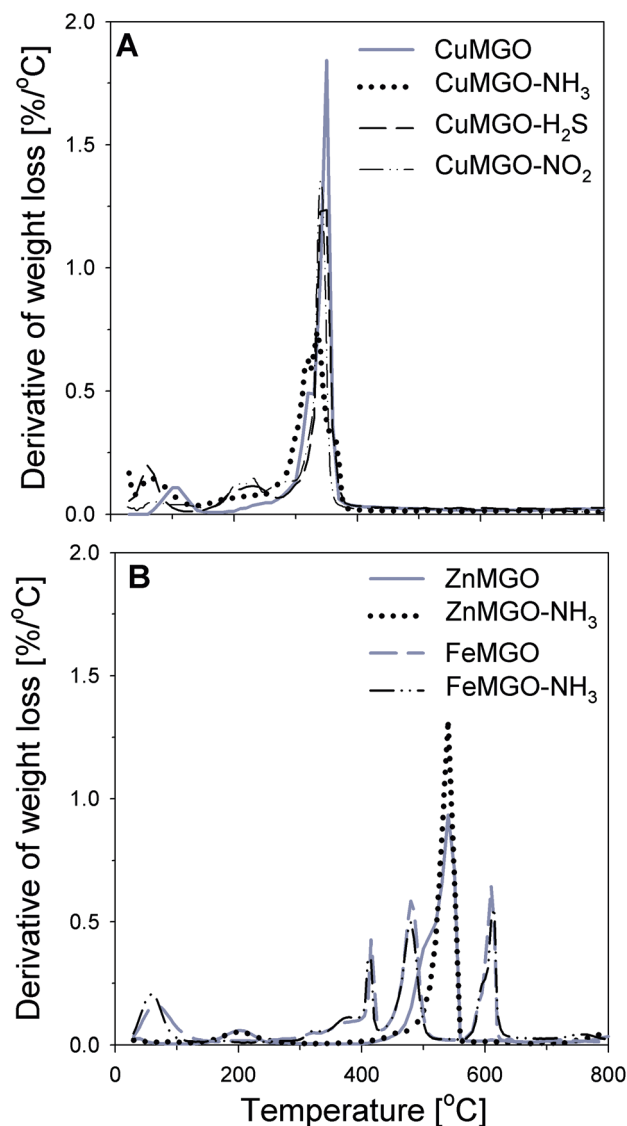


Fig. 6 DTG curves in nitrogen for the initial and exposed samples: (A) Cu-based composites, and (B) Zn- and Fe-based composites.

related to the decomposition of the organic ligands as well as the decrease in its intensity. This may indicate the presence in the exposed samples of several forms of BTC such as BTC within HKUST-1 network or “free” BTC molecules. On the contrary, there is no visible change in thermal stability for the Zn- and Fe-based composites.

Additional evidence of the reactions between the adsorbates and the metallic centers, resulting in the release of the organic ligands, is provided by the porosity measurements of the exposed samples (Table 2).^{17,24,25,27} NH_3 , H_2S and NO_2 adsorptions caused a significant decrease in the porosity of Cu-based materials ranging from 60 to 90%, depending on the adsorbate, which directly supports the partial collapse of the MOF component. The degradation of the materials is the consequence of the release of the ligands. The instability of Cu-based MOFs in the presence of N-containing molecules has already been reported⁵⁷ and, overall the coordination of N- and S-containing molecules to Cu atoms could be expected taking into account the

chemistry of copper. On the contrary, the porosity of ZnMGO and FeMGO is mostly preserved after ammonia adsorption, showing that NH_3 did not react with the framework in a way that would release the organic ligand and cause the collapse of the MOF. This is in accordance with the FT-IR results presented above.

Considering all the results, the different steps of the reactive adsorption of NH_3 , H_2S and NO_2 on the Cu-based materials are summarized in Fig. 7. The molecules first coordinate to the Cu sites inducing a color change of the adsorbent. Further reaction with the frameworks weakens the Cu–O coordination between the metallic sites and the organic ligands and leads to the formation of new copper salts, $\text{Cu}(\text{NH}_3)_4^{2+}$, CuS and $\text{Cu}(\text{NO}_3)_2$, and causes the release of the organic ligands. The latter step induces a second color change except in the case of NO_2 adsorption. This is likely due to the similar color of $\text{Cu}(\text{NO}_3)_2$ to that of the previously formed compound. In the case of Fe-based materials,

Table 2 Parameters of the porous structure calculated from nitrogen adsorption isotherms at $-196\text{ }^\circ\text{C}$

Sample	S_{BET} ($\text{m}^2 \text{g}^{-1}$)	V_t ($\text{cm}^3 \text{g}^{-1}$)	V_{mic} ($\text{cm}^3 \text{g}^{-1}$)
ZnMGO	806	0.416	0.388
ZnMGO– NH_3	807	0.415	0.388
CuMGO	1002	0.527	0.478
CuMGO– NH_3	115	0.060	0.058
CuMGO– H_2S	406	0.267	0.195
CuMGO– NO_2	159	0.251	0.189
FeMGO	1172	0.600	0.501
FeMGO– NH_3	1061	0.563	0.439

the predominant reactive adsorption mechanism is the acid–base reaction between ammonia and the water molecules already coordinated to the metallic sites. In the case of the Zn-based materials, hydrogen bonds are formed between ammonia and the oxygen atoms of the ZnO_4 tetrahedra units of MOF-5.

The effect of water on the adsorption of NH_3 and NO_2 on the studied MOFs and composites is an important aspect of gas adsorption in real-life applications especially when moisture is present in the challenge stream. The impact of water was studied previously and the interested reader is directed towards those papers for detailed information.^{23,25–27,58} Briefly, it was found that water enhances NH_3 adsorption on Cu-based MOFs and derived composites *via* dissolution of NH_3 in the water film.^{23,27} This effect was also observed for the adsorption of NH_3 on MOF-5 and ZnMGO but it was counterbalanced by the collapse of the MOF structure caused by hydrogen-bonding between the water molecules and the zinc oxide tetrahedra.⁵⁸ Finally, competitive adsorption of water and NH_3 or NO_2 was observed on FeMGO and CuMGO, respectively.^{25,26}

Conclusions

The results of this study indicate that MOF metallic sites coordinate with the GO oxygen groups to form new composites with distinct properties compared to those of the parent materials. In particular, depending on the structure of the MOF, such interactions can induce the formation of a new pore space in the interface between the carbon layers and the MOF units. This phenomenon is responsible for the enhanced adsorption capacity

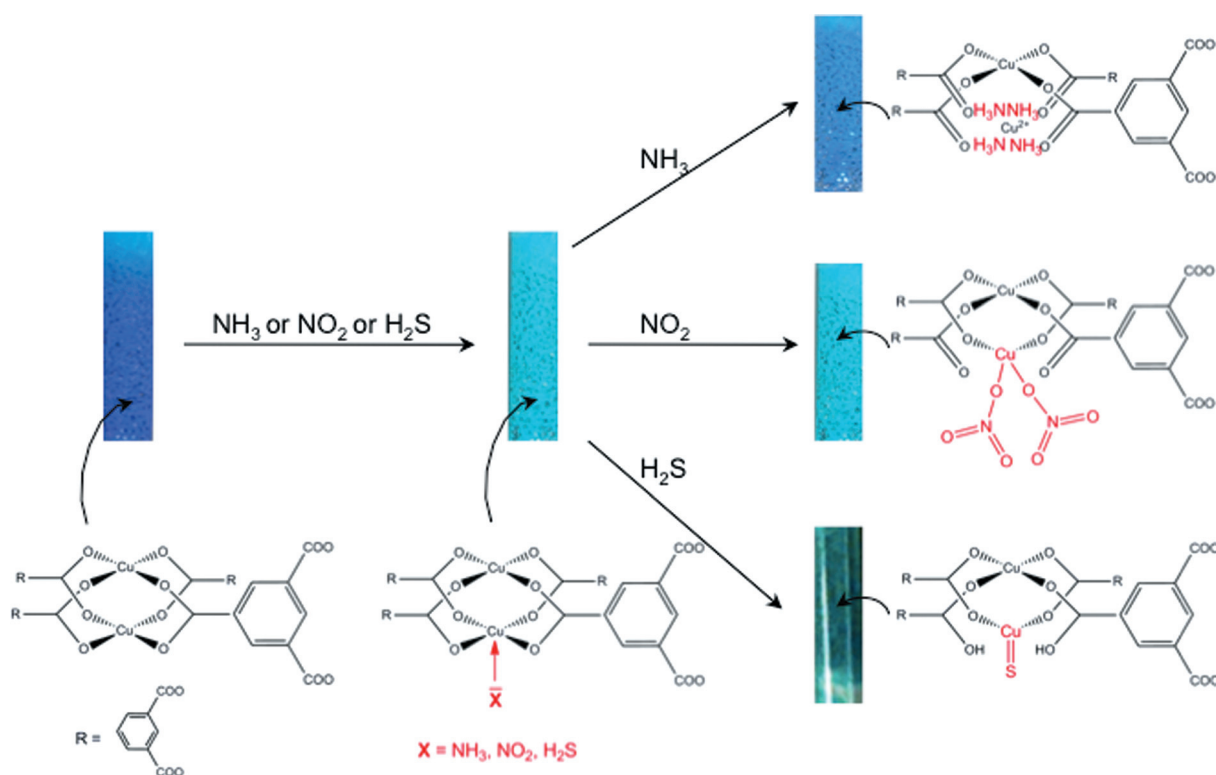


Fig. 7 Schematic of the adsorption process of NH_3 , H_2S and NO_2 on the Cu-based materials with evidence of the color changes and the identification of the reactions products.

of the toxic gases compared to that of the parent materials. In addition to the physisorption mechanism, the reactive adsorption of NH₃, H₂S and NO₂ also takes place. First, the lone pair of electron on these species enables their coordination to the MOFs' unsaturated metallic sites as in HKUST-1. This phenomenon weakens the bonds between the metallic sites and the organic ligands of the MOFs and leads to the release of the metals and organic ligands. As a result, the adsorbates further react with the metals and the formation of Cu(NH₃)⁴⁺, CuS and Cu(NO₃)₂ is proposed, depending on the adsorbate. This process also causes the decomposition of the framework with a significant loss in the porosity. For the MIL- and MOF-5-derived materials, which do not contain unsaturated metallic sites, the predominant adsorption mechanisms, besides physisorption, are the acid–base reaction and hydrogen bonding, respectively. Since the latter processes are not destructive, the frameworks retain their original porosity.

Acknowledgements

This work was supported by ARO (Army Research Office) grant W911NF-10-1-0030 and NSF collaborative grant 0754945/0754979. The input of Dr Levasseur and Ms Barbara Mendoza is appreciated.

References

- U. Müller, M. M. Schubert and O. M. Yaghi, in *Handbook of Heterogeneous Catalysis*, ed. U. Müller, M. M. Schubert and O. M. Yaghi, Wiley-VCH Verlag GmbH & Co. KGaA, Weinheim, Germany, 2008.
- P. Wright, in *Microporous Framework Solids*, ed. J. A. Connor, RSC Publishing, Cambridge, UK, 2008.
- S. L. James, *Chem. Soc. Rev.*, 2003, **32**, 276–288.
- A. U. Czaja, N. Trukhan and U. Müller, *Chem. Soc. Rev.*, 2009, **38**, 1284–1293.
- P. Horcajada, C. Serre, M. Vallet-Regí, M. Sebban, F. Taulelle and G. Férey, *Angew. Chem., Int. Ed.*, 2006, **45**, 5974–5978.
- B. Chen, L. Wang, F. Zapata, G. Qian and E. B. Lobkovsky, *J. Am. Chem. Soc.*, 2008, **130**, 6718–6719.
- B. Chen, L. Wang, Y. Xiao, F. R. Fronczek, M. Xue, Y. Cui and G. Qian, *Angew. Chem., Int. Ed.*, 2009, **48**, 500–503.
- A. Lan, K. Li, H. Wu, D. H. Olson, T. J. Emge, W. Ki, M. Hong and J. Li, *Angew. Chem., Int. Ed.*, 2009, **48**, 2334–2338.
- P. Mahata, S. Natarajan, P. Panissod and M. Drillon, *J. Am. Chem. Soc.*, 2009, **131**, 10140–10150.
- B. V. Harbuzaru, A. Corma, F. Rey, P. Atienzar, J. L. Jordá, H. García, D. Ananias, L. D. Carlos and J. Rocha, *Angew. Chem., Int. Ed.*, 2008, **47**, 1080–1083.
- H. K. Chae, D. Y. Siberio-Perez, J. Kim, Y. Go, M. Eddaoudi, A. J. Matzger, M. O'Keeffe and O. M. Yaghi, *Nature*, 2004, **427**, 523–527.
- D. Britt, D. Tranchemontagne and O. M. Yaghi, *Proc. Natl. Acad. Sci. U. S. A.*, 2008, **105**, 11623–11627.
- J. G. Vitillo, L. Regli, S. Chavan, G. Ricchiardi, G. Spoto, P. D. C. Dietzel, S. Bordiga and A. Zecchina, *J. Am. Chem. Soc.*, 2008, **130**, 8386–8396.
- A. C. McKinlay, B. Xiao, D. S. Wragg, P. S. Wheatley, I. L. Megson and R. E. Morris, *J. Am. Chem. Soc.*, 2008, **130**, 10440–10444.
- D.-C. Zhong, J.-B. Lin, W.-G. Lu, L. Jiang and T.-B. Lu, *Inorg. Chem.*, 2009, **48**, 8656–8658.
- A. Demessence, D. M. D'Alessandro, M. L. Foo and J. R. Long, *J. Am. Chem. Soc.*, 2009, **131**, 8784–8786.
- C. Petit and T. J. Bandoz, *Adv. Funct. Mater.*, 2010, **20**, 111–118.
- M. Jahan, Q. Bao, J.-X. Yang and K. P. Loh, *J. Am. Chem. Soc.*, 2010, **132**, 14487–14495.
- O. Shekka, N. Roques, V. Mugnaini, C. Munuera, C. Ocal, J. Veciana and C. Woll, *Langmuir*, 2008, **24**, 6640–6648.
- S. Hermes, D. Zacher, A. Baunemann, C. Wöll and R. A. Fischer, *Chem. Mater.*, 2007, **19**, 2168–2173.
- C. Petit and T. J. Bandoz, *Adv. Mater.*, 2009, **21**, 4753–4757.
- C. Petit, J. Burrez and T. J. Bandoz, *Carbon*, 2011, **49**, 563–572.
- C. Petit, B. Mendoza and T. J. Bandoz, *Langmuir*, 2010, **26**, 15302–15309.
- C. Petit, B. Mendoza and T. J. Bandoz, *ChemPhysChem*, 2010, **11**, 3678–3684.
- B. Levasseur, C. Petit and T. J. Bandoz, *ACS Appl. Mater. Interfaces*, 2010, **2**, 3606–3613.
- C. Petit and T. J. Bandoz, *Adv. Funct. Mater.*, 2011, **21**, 2108–2117.
- C. Petit, B. Mendoza, D. O'Donnell and T. J. Bandoz, *Langmuir*, 2011, **27**, 10234–10242.
- W. S. Hummers and R. E. Offeman, *J. Am. Chem. Soc.*, 1958, **80**, 1339–1339.
- M. Seredych and T. J. Bandoz, *J. Phys. Chem. C*, 2007, **111**, 15596–15604.
- H. Li, M. Eddaoudi, M. O'Keeffe and O. M. Yaghi, *Nature*, 1999, **402**, 276–279.
- S. S.-Y. Chui, S. M.-F. Lo, J. P. H. Charmant, A. G. Orpen and I. D. Williams, *Science*, 1999, **283**, 1148–1150.
- A. R. Millward and O. M. Yaghi, *J. Am. Chem. Soc.*, 2005, **127**, 17998–17999.
- P. Horcajada, S. Surble, C. Serre, D.-Y. Hong, Y.-K. Seo, J.-S. Chang, J.-M. Greneche, I. Margiolaki and G. Férey, *Chem. Commun.*, 2007, 2820–2822.
- T. Bandoz, *Activated Carbon Surfaces in Environmental Remediation*, Academic Press, Oxford, UK, 2006, pp. 231–292.
- N. Shirahama, S. H. Moon, K. H. Choi, T. Enjoji, S. Kawano, Y. Korai, M. Tanoura and I. Mochida, *Carbon*, 2002, **40**, 2605–2611.
- W.-J. Zhang, A. Bagreev and F. Rasouli, *Ind. Eng. Chem. Res.*, 2008, **47**, 4358–4362.
- S. Brunauer, P. H. Emmett and E. Teller, *J. Am. Chem. Soc.*, 1938, **60**, 309–319.
- J. H. de Boer, B. C. Lippens, B. G. Linsen, J. C. P. Broekhoff, A. van den Heuvel and T. J. Osinga, *J. Colloid Interface Sci.*, 1966, **21**, 405–414.
- A. Buchsteiner, A. Lerf and J. Pieper, *J. Phys. Chem. B*, 2006, **110**, 22328–22338.
- C. Hontoria-Lucas, A. J. López-Peinado, J. d. D. López-González, M. L. Rojas-Cervantes and R. M. Martín-Aranda, *Carbon*, 1995, **33**, 1585–1592.
- H. K. Jeong, *et al.*, *J. Phys. D: Appl. Phys.*, 2009, **42**, 065418.
- L. Huang, H. Wang, J. Chen, Z. Wang, J. Sun, D. Zhao and Y. Yan, *Microporous Mesoporous Mater.*, 2003, **58**, 105–114.
- Y.-K. Seo, G. Hundal, I. T. Jang, Y. K. Hwang, C.-H. Jun and J.-S. Chang, *Microporous Mesoporous Mater.*, 2009, **119**, 331–337.
- A. Vimont, J.-M. Goupil, J.-C. Lavalley, M. Daturi, S. Surblé, C. Serre, F. Millange, G. Férey and N. Audebrand, *J. Am. Chem. Soc.*, 2006, **128**, 3218–3227.
- S. C. Ndlela and B. H. Shanks, *Ind. Eng. Chem. Res.*, 2003, **42**, 2112–2121.
- H. H. F. M. Lerf A and J. Klinowski, *J. Phys. Chem. B*, 1998, **102**, 4477.
- J. C. Thompson, *Phys. Rev. A*, 1971, **4**, 802–804.
- D. Uhlmann, S. Smart and J. C. Diniz da Costa, *J. Membr. Sci.*, 2011, **380**, 48–54.
- C. Petit, M. Seredych and T. J. Bandoz, *J. Mater. Chem.*, 2009, **19**, 9176–9185.
- J. Helminen, J. Helenius, E. Paatero and I. Turunen, *J. Chem. Eng. Data*, 2001, **46**, 391–399.
- T. J. Bandoz and C. Petit, *J. Colloid Interface Sci.*, 2009, **338**, 329–345; S. Vairam and S. Govindarajan, *Thermochim. Acta*, 2004, **414**, 263–270.
- Infrared and Raman Spectra of Inorganic and Coordination Compounds, Applications in Coordination, Organometallic, and Bioinorganic Chemistry*, ed. K. Nakamoto, Wiley, Hoboken, NJ, 2009, pp. 62–67.
- N. I. Kovtyukhova, P. J. Ollivier, B. R. Martin, T. E. Mallouk, S. A. Chizhik, E. V. Buzaneva and A. D. Gorchinskiy, *Chem. Mater.*, 1999, **11**, 771–778.
- S. Hermes, F. Schroder, S. Amirjalayer, R. Schmid and R. A. Fischer, *J. Mater. Chem.*, 2006, **16**, 2464–2472.
- E. Biemmi, T. Bein and N. Stock, *Solid State Sci.*, 2006, **8**, 363–370.
- D. R. Lide, *CRC Handbook of Chemistry and Physics*, ed. D. R. Lide, CRC Press, Boca Raton, FL, 1993.
- G. W. Peterson, G. W. Wagner, A. Balboa, J. Mahle, T. Sewell and C. J. Karwacki, *J. Phys. Chem. C*, 2009, **113**, 13906–13917.
- C. Petit and T. J. Bandoz, *Adsorption*, 2011, **17**, 5–16.